LAWRENCE
LIVERMORE
NATIONAL
LABORATORY

UCRL-CONF-153850

Magnetorheological Finishing for Imprinting Continuous Phase Plate Structure onto Optical Surfaces

J. A. Menapace, S. N. Dixit, F. Y. Génin, and W. F. Brocious

January 5, 2004

Boulder Damage Symposium XXXV, Boulder, Colorado, September 21-24, 2003

Updated October 14, 2003

Magnetorheological Finishing for Imprinting Continuous Phase Plate Structure onto Optical Surfaces

Joseph A. Menapace[a], Sham N. Dixit[a], Francois Y. Génin[a], and Wayne F. Brocious
[a]University of California, Lawrence Livermore National Laboratory,
7000 East Avenue L-491, Livermore, CA 94550

ABSTRACT

Magnetorheological finishing (MRF) techniques have been developed to manufacture continuous phase plates (CPP's) and custom phase corrective structures on polished fused silica surfaces. These phase structures are important for laser applications requiring precise manipulation and control of beam-shape, energy distribution, and wavefront profile. The MRF's unique deterministic-sub-aperture polishing characteristics make it possible to imprint complex topographical information onto optical surfaces at spatial scale-lengths approaching 1 mm. In this study, we present the results of experiments and model calculations that explore imprinting two-dimensional sinusoidal structures. Results show how the MRF removal function impacts and limits imprint fidelity and what must be done to arrive at a high quality surface. We also present several examples of this imprinting technology for fabrication of phase correction plates and CPPs for use at high fluences.

Keywords: Continuous phase plate, diffractive optics, Magnetorheological finishing, MRF, irradiance

INTRODUCTION

The National Ignition Facility (NIF) Project at Lawrence Livermore National Laboratory (LLNL) is developing Magnetorheological Finishing (MRF) as an advanced polishing technique to accurately imprint complex topographical patterns onto optical surfaces. The most interesting and direct application of this advanced technology is its use in the manufacture of small- and large-aperture custom continuous phase plates (CPP's). Several of the experimental campaigns planned for NIF call for specific target plane laser beam characteristics incorporating well-defined beam-shapes, energy distributions, and wavefront profiles[1,2]. Custom CPP's can be used in the seed laser portion or, preferably, in the final portion of NIF's main laser beam optical system to provide for precise manipulation and control of these characteristics to fulfill NIF experimental requirements[2]. Additionally, CPP's can be used for correcting or homogenizing target plane aberrations and hot spots arising from other optics present in the beamline.

Prior work on large-aperture high-power laser system phase plate manufacture linked mask and etch technologies to imprint phase manipulating patterns onto optics. Early efforts on lower efficiency forerunners of the CPP utilized a masking and acid wet etching approach to imprint binary[3,4] (rectangular/hexagonal phase plates) and 16 level step patterns[5,6] (kinoform phase plate) onto fused silica surfaces. More recently, masking and resistive ion etching techniques were used to imprint highly efficient CPP patterns for use at the Laboratory for Laser Energetics[7] and the Laser Megajoule facility[8]. In contrast, MRF offers a direct method for imprinting topographical features onto optics without the use of masks or master plates because of its deterministic polishing capability and close interplay with interferometry. The MRF process provides for a high level of versatility and speed in CPP manufacture as topographical polishing can be conducted by directly combining computer generated CPP and/or interferometric profiles with large MRF volumetric removal rates. Additionally, the process seamlessly fits into the advanced manufacturing process technology we are currently refining for production of large-aperture optical components possessing high ultraviolet damage resistance[9].

In this study, we present the results of our MRF process development as it pertains to CPP imprinting feasibility and manufacture. First, we summarize the results of diagnostic experiments conducted using a set of prescribed two-dimensional sinusoidal topographical functions that were imprinted onto fused silica substrates. These tests show the feasibility of using MRF to perform CPP imprinting. We then discuss the results of imprinting a small-aperture CPP that

was recently used on NIF for target diagnostic experiments. The imprinting of this CPP incorporates the developments and observations made during the diagnostic experiments.

DIAGNOSTIC TESTS USING TWO-DIMENSIONAL SINUSOIDAL PATTERNS

The fundamentals of MRF finishing have been previously described[9-19] so they will not be discussed in detail here. Two pertinent aspects to the imprinting process, however, deserve mention. First, a key feature in the MRF process is the size and shape of the removal function used to perform the polishing, Figure 1. The deterministic nature of the MRF process makes it possible to correct optic figure over a large area using a small controllable removal function. In its normal operating configuration, MRF uses the removal function and dwell time to differentially remove material from areas of an optic so that the desired surface or wavefront properties are obtained.[9,10] Typically this process is used to improve the flatness of plano parts and to fine-tune spherical or aspherical character on focusing optics. These corrections are long-range compared to the size of the removal function. Imprinting of surface topography onto an optical surface such as that required for CPP's is a non-traditional application of this technology. The distinct difference is that instead of removing the waviness or imperfections from the optical surface, MRF is applying surface structure in a deterministic fashion. For short spatial periods, one can think of the process as imprinting or correcting a number of small lenses present on a large piece of glass. Here, the size of the removal function becomes important in attaining the desired topographical fidelity.

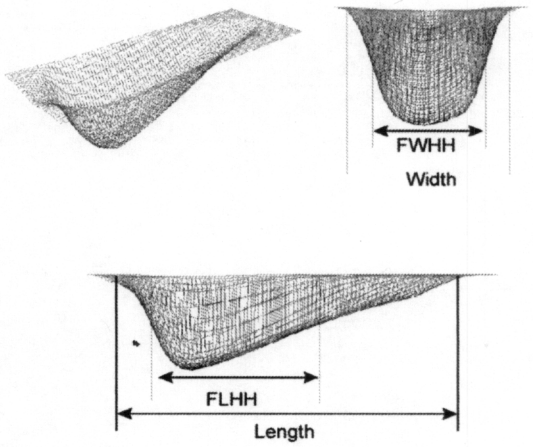

Figure 1: The MRF removal function possesses a distinct size and shape. The width and the length of the removal function are important for topographical imprinting. Full width at half height (FWHH) and full length at half height (FLHH) are the metrics used to define the removal function.

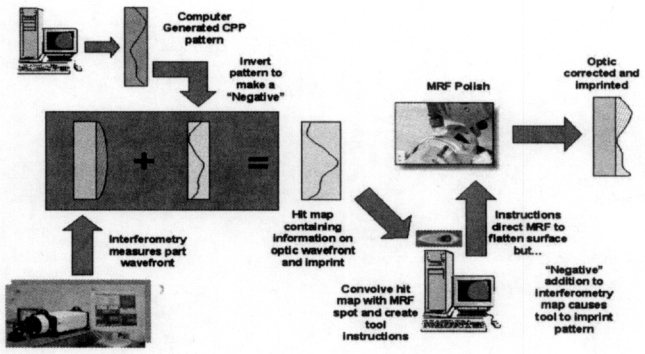

Figure 2: MRF imprinting process schematic. Interferometry, computer generated prescriptions, and software work together to create machine instructions to deterministically enable topographical imprinting.

Second, the MRF process integrates interferometry or user/computer generated surface topographical information and computer algorithms to generate the required instrument stage motions to deterministically polish material surfaces, Figure 2. The MRF system software provides the mechanism to perform this task by using a solving algorithm that performs a deconvolution of the removal function shape and the incoming surface structure measured via interferometry or mathematically supplied by the user. In a typical raster-polishing application, the MRF software uses the existing surface figure as a starting point and a flat surface as the desired end-point. The algorithm attempts to converge to a solution that minimizes the rms of the surface via the removal function/existing surface deconvolution. For imprinting, the process must be inverted. It must start with a flat surface (or existing surface figure) and end with a surface possessing desired topography. This is accomplished by adding the height-inverted topographical imprint map (negative image) to the starting metrology (Figure 2). The solving algorithm converges this virtual surface towards flatness. This results in the proper removal of material from the initial optical surface even though the software output is a plano surface.

To test the MRF instrument's ability to imprint topography onto optical surfaces, two-dimensional sinusoidal waves were generated with specified amplitude, phase, and various spatial periods in a square map array compatible for direct input into the MRF system software. The two-dimensional sinusoidal waves have the analytic form (1):

$$f(x,y) = A \sin\left(\frac{2\pi}{T}x + \varphi_x\right) \sin\left(\frac{2\pi}{T}y + \varphi_y\right) \quad (1)$$

A = *amplitude*

T = *spatial period*

φ = *phase*

Sinusoidal waves represent simple and continuous surface topographies that can be generated using a minimum number of shape defining parameters. They have several advantages that make them acceptable for use in studying the MRF topographical imprinting process. First, their periodic structure can be easily measured and analyzed using interferometry and interpreted in terms of amplitude, period, and phase. Second, model surfaces can be readily created using the functions that can be mathematically compared to the imprinted surfaces to study feature shape, amplitude, slope, and periodic behavior. The functions can also be analytically manipulated to determine key features such as gradient at critical points and metrics such as root mean square, rms or R_q, and mean amplitude, R_a.[20] Lastly, detailed comparisons can be made showing differences between raster and step directions of motion during MRF finishing.

Two experiments were designed and executed to investigate the relationship between the physical characteristics of the MRF removal function and the accuracy/ability to imprint surface features of various sizes. The first experiment involved using a constant removal function size and shape to produce two-dimensional sinusoidal wave imprints with variable spatial periods. These experiments were used to compare the predicted peak-to-valley (PV) and rms to the experimentally measured values. The results determine the limitations of the process as the spatial periods become smaller. In the second experiment, a fixed two-dimensional sinusoidal spatial period pattern was imprinted onto a surface using removal functions of varying sizes, some smaller than the spatial period, some similar to the spatial period, and some larger than the spatial period. In this situation, topographical deviations from the prescribed surface profile can be evaluated as a function of removal function size. A 30-mm square area was selected to imprint two-dimensional sinusoidal waves onto the surface of fused silica. The PV of the sinusoidal waves was chosen at 0.5 μm. The imprint patterns were introduced to the MRF tool using the QED two-dimensional surface profile format.[21] Prior to imprinting, the fused silica optics were polished and corrected for surface wavefront to about 60 nm PV. The optical surfaces were assumed perfectly flat for the topographical imprinting; hence, no wavefront correction was incorporated into the prescription used (see Figure 2).

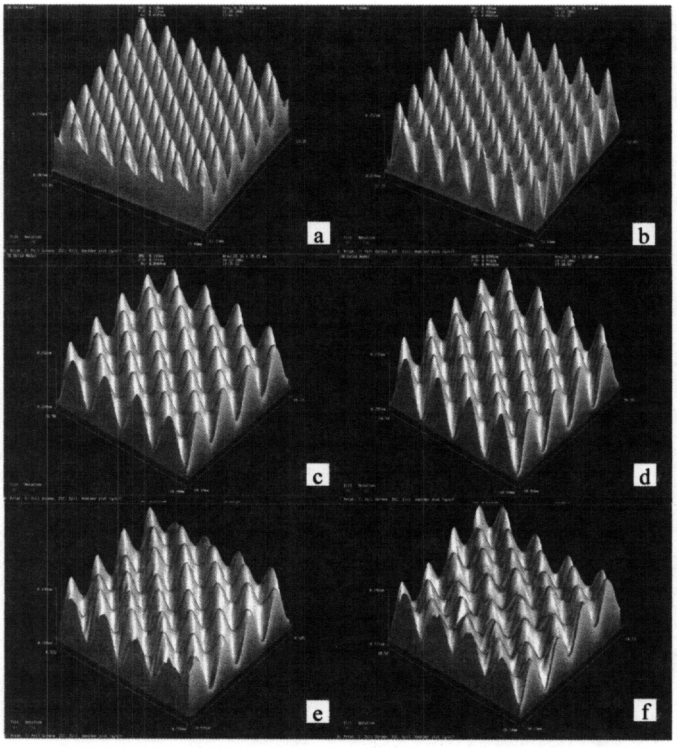

Figure 3: Experimental 5-mm sinusoidal profiles after MRF imprinting using removal function FWHH a) 1.7-mm, b) 2.1-mm, c) 2.8-mm, d) 3.6-mm, e) 4.8-mm, and f) 7.1-mm.

Constant spatial period imprinting using variable removal function sizes

For the first sinusoidal wave experiment, six removal functions with widths of 1.7-, 2.1-, 2.8-, 3.6-, 4.8-, and 7.1-mm were used to cover the range

of sizes around the 5-mm sinusoidal period. The pertinent data for the software convergences for these sinusoidal imprints are listed in Table 1. Figure 3 shows the experimental sinusoidal profiles after MRF imprinting.

Table 1: MRF software convergence results for a 5-mm sinusoidal wave imprinted onto fused silica using various removal function sizes.

Imprint	*Removal Function Width (FWHH) (mm)*	*PV before conv. (μm)*	*rms before conv. (μm)*	*PV after conv. (μm)*	*rms after conv. (μm)*
a	1.65	0.5	0.125	0.077	0.0072
b	2.06	0.5	0.125	0.124	0.0153
c	2.75	0.5	0.125	0.099	0.0109
d	3.58	0.5	0.125	0.107	0.0142
e	4.84	0.5	0.125	0.256	0.0525
f	7.12	0.5	0.125	0.208	0.0436

For the patterns imprinted using removal functions with FWHH less than two-thirds the 5-mm spatial period (Figure 3a-d), the two-dimensional sinusoidal patterns are close to those prescribed. The patterns imprinted with removal function dimensions greater than the Nyquist limit (Figure 3e-f) show significant efficiency degradation due to aliasing and bandwidth limiting. This is particularly apparent in the imprint in Figure 3f. The correlation and trend imply that the efficiency of the MRF process in imprinting surface topography is directly tied to, and limited by, the removal function size. Thus, the removal function dimensions essentially limit the bandwidth of the sampling of the surface topography due to Nyquist critical sampling issues. Simply put, the smallest portion of the removal function must be at least half the shortest spatial period to be imprinted. For experimental work, the operator can use the FWHH of the removal function. With this strategy, the removal function width at FWHH should be smaller than two-thirds that of the shortest spatial period to be imprinted. Trying to imprint shorter spatial periods (higher frequencies) than the smallest practical removal function dimensions (critical frequency) results in aliasing since these spatial periods are spuriously moved into spatial periods longer than the critical period. The removal function contains a band of critical sampling frequencies between its narrowest and widest footprint dimensions. This qualitatively explains the behavior of the convergences as the spatial periods decrease. In these instances, less and less of the removal function is effectively used for imprinting the topography. This leads to longer polishing times and greater material removal due to "collateral" polishing. We define collateral polishing as imprinting that occurs due to some portion of the removal function that cannot effectively perform the desired material removal to obtain the topographical shape. This "ineffective portion" corresponds to the shallow portions of the removal function footprint. This polishing spoils the imprinting efficiency and results in an increase in uniform material removal to attain the desired topography.

To gain a better understanding of the quality of the imprinting, the surface interferometry was numerically fit to the sinusoidal prescriptions, equation 1, using the rms difference between the actual surface topography and the parameterized prescription as a minimization metric. Prior to analyzing the difference between theoretical and experimental surface profiles, the sinusoidal wave amplitude, X and Y spatial periods, X and Y phases, and relative orientation of the prescription and interferometry were adjusted to achieve the best fit to the experimental data. Even though, phases are set to zero in the prescription, they are used in the fitting since the metrology is clipped to remove edge effects and MRF tool turn-around artifacts from the data. The phases also ensure that the computed PV and rms of the model surfaces correlate to surface metrology. The minimized parameters for the modeled two-dimensional sinusoidal waves are listed in Table 2.

The results presented in Table 2 show that the topographical imprinting closely reproduces the desired 5.0-mm spatial period within the lateral measurement resolution of the interferometry used to measure the parts. The interferometry resolution used for measurement was 0.133 mm/pixel. The magnification was set to maximize the image size of the surface being imprinted. The corresponding PV and rms for each of the fits are included in Table 3 along with the measured interferometric data. Comparison of the experimental and the best-fit surfaces, using a point-by-point and a statistical basis, provides useful information regarding the quality of the imprinting. First, it indicates that the topography follows the prescription shape very closely even though the desired amplitude is not achieved (Tables 2 and 3). For example, the profile imprinted using 2.8-mm removal function Figure 4a, compares quite well with the model surface, Figure 4b, as implied by the difference between the two surfaces, Figure 4c. In this case the rms of the part is within 0.8

Table 2: Numerical fitting parameters for the two-dimensional sinusoidal waves fit to the experimentally imprinted topographies.

Imprint	*Amplitude (μm)*	*X Period (mm)*	*X Phase (rad)*	*Y Period (mm)*	*Y Phase (rad)*	*X/Y Rotation (deg)*
a	0.235	5.002	0.254	5.071	-2.260	0.232
b	0.210	5.029	0.762	5.117	-0.817	-0.905
c	0.236	5.038	1.533	5.088	-1.004	0.231
d	0.197	5.075	1.288	5.101	-1.005	0.514
e	0.096	4.994	1.536	5.191	-0.885	0.500
f	0.124	5.103	1.476	5.081	-0.654	-1.750

Table 3: Surface characteristics for the imprinted two-dimensional topographies and the numerically fit sinusoidal waves.

Imprint	*Part PV (μm)*	*Sine Wave PV (μm)*	*Part rms (μm)*	*Sine Wave rms (μm)*
a	0.532	0.470	0.1204	0.1182
b	0.496	0.421	0.1094	0.1068
c	0.555	0.471	0.1191	0.1182
d	0.442	0.394	0.0998	0.0991
e	0.317	0.191	0.0535	0.0477
f	0.306	0.248	0.0631	0.0612

percent of the corresponding model value. The rms of the difference between the experimental and the model topographies is 12 nm, which indicates that the average difference between the part and the prescription is less than 2.5 percent on average. The rms also implies that, at most, 11 percent of the topography deviates by, at most, 36 nm, from the model (Chebyshev inequality).[22] Errors from the interferometry also contribute to the topographical analysis quality, as vertical dimension errors can reach 50 nm due to the topographical slopes and the 0.133-mm/pixel interferometry lateral resolution used.

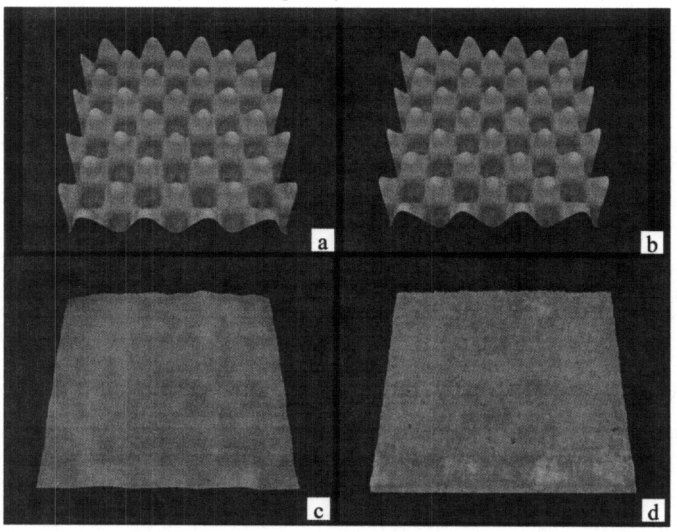

Figure 4: Comparison of the experimental sinusoidal profile with the modeled profile for imprinting conducted using a 2.8-mm removal function. a) Experimental surface topography, b) modeled surface, c) difference between the experimental and modeled surface, and d) the optical surface before MRF imprinting. The surface topography follows the substrate surface topography during imprinting. The portions of the imprint that are missing follow the sinusoidal pattern - see c).

Second, the imprinting error mainly stems from minor mismatches near the peaks and valleys. The mismatches in the imprint appear to follow the sinusoidal imprint pattern, Figure 4c. This is equivalent to slight "boxcar" smoothing of the peaks and valleys by the removal function where collateral polishing causes feature washout in areas where slope topographical slope changes are large.

Third, the imprinting follows the existing topography of the substrate. Comparison of the difference map, Figure 4c, and the surface prior to imprinting, Figure 4d, shows that the patterns are imprinted upon long-range features that exist in the surface prior to MRF imprinting. The substrate possessed a PV of 45 nm, and a rms of 3.1 nm, which implies that about 25 percent of the topography errors can be due to error propagation from the substrate. This can be corrected by incorporating the substrate interferometry before imprinting the prescription, (Figure 2). The test imprints were performed assuming that surfaces were perfectly flat and thus did not contain initial surface structure information.

For all the 5-mm sinusoidal patterns imprinted, the desired amount of material removal during a single MRF run was never reached; hence the PV and rms values fall short of their expected values. On average the inferred PV's for the patterns imprinted using removal functions smaller than the 5-mm spatial period was 88 - 90 percent of the desired PV. This is consistent with the observations noted during modeling. One pass over the optic is therefore insufficient to reach the desired surface topography for high precision work. The experiments show that PV not a good metric to assess the quality of the imprinting. Since PV is computed from only two data points out of possible thousands available, the optic appears worse than it actually is. The rms calculated from all the data on the optical surface and can give a better indication of the overall optic performance, as shown in Figure 5 and Tables 1 and 3. For the two-dimensional sinusoidal waves imprinted, the topographical accuracy is good when compared to the best-fit profiles. The major difference between the experimental and prescribed profiles is directly attributable to the shortfall in peak amplitude and the amount of material removed. Scaling the imprint topography to the desired prescription depth based upon the measured rms indicates that the quality would be as expected, in the vicinity of rms = 0.125 μm.

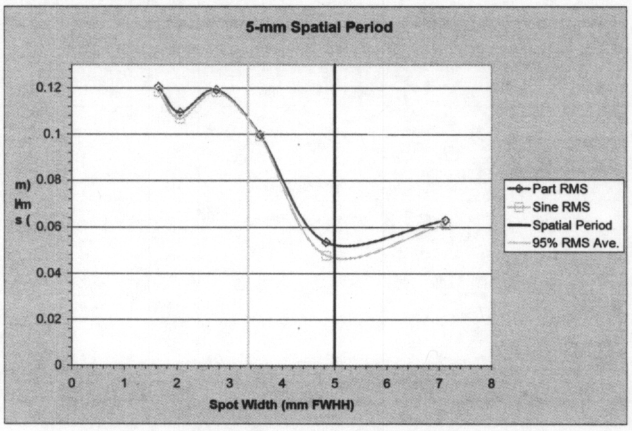

Figure 5: Computed and measured rms's for the 5-mm imprints as a function of removal function size. Quality is high for small spots. Rms deteriorates as the removal function size approaches the topographical spatial period. Taking 5 % deterioration in the average rms as a metric on the imprints performed with small spots, a critical spot size of 2/3 the spatial period is obtained.

The rms for each of the imprints form a trend with removal function size, Figure 5. The plots show that this metric remains high for removal function sizes below the topographical spatial period and deteriorate when the removal function size approaches or exceeds the spatial period. This was predicted during convergence modeling for which the imprinting deteriorated and failed when the spatial period approached the same size as the smallest removal function dimension. If one assumes that imprinting is satisfactory to 95 percent of its average rms value for the small removal function imprints, Figure 3a-d, the intersection of this point and the removal function width on the plots yields the "two-thirds rule". This rule suggests that effective imprinting can be achieved using a removal function size that is less than approximately two-thirds the size of the shortest spatial period in the topography. Furthermore, between this and the critical Nyquist size, the effectiveness of the imprinting significantly deteriorates.

Constant removal function size and variable period

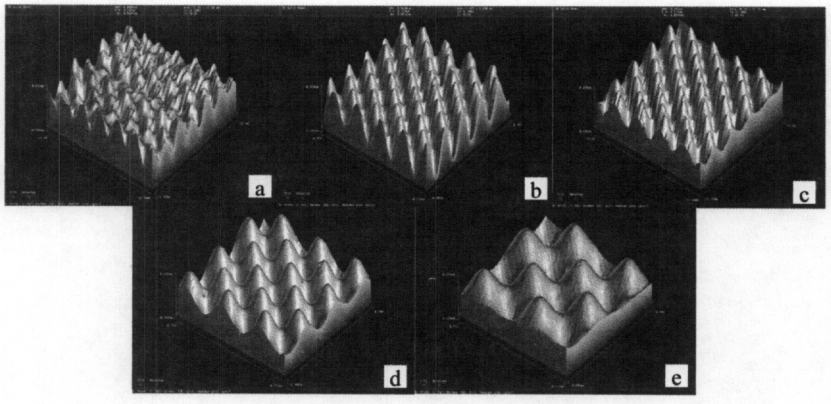

Figure 6: Experimental surface profiles of the three-dimensional sinusoidal waves with a) 3.75-mm, b) 5-mm, c) 6.67-mm, d) 10-mm and e) 15-mm spatial periods on 30-mm squares imprinted with a 5.6 mm removal function.

A complementary experiment to the 5-mm two-dimensional sinusoidal wave imprinting was conducted on fused silica samples. The experiments involved keeping the removal function size constant at 5.6 mm and imprinting patterns varying from 3.75-, 5-, 6.67-, 10- and 15-mm spatial periods. The pertinent data for the convergences pertaining to these imprints are listed in Table 8. Figure 6 shows the experimental sinusoidal profiles after MRF imprinting. The results of the topographical imprinting for this experiment corroborate the findings from the complementary experiment where the spatial period was held constant and the removal function size

was varied. Namely, for topographies with a 15.0-, 10.0-, and 6.67-mm spatial period imprinted using a fixed size removal function are accurate until the spatial period approaches the dimensions of the removal function at 5.0- and 3.75-mm spatial period. At this point, the topography efficiency deteriorates and feature scrambling occurs from aliasing and bandwidth limiting. Aliasing and period scrambling are particularly apparent in the 3.75-mm spatial period imprint that is beyond the removal function's ability to imprint effectively, Figure 6a.

Table 4: Numerical fitting parameters for the two-dimensional sinusoidal waves fit to the experimentally imprinted topographies, 4.63 mm FWHH removal function.

Imprint	*Amplitude (μm)*	*X Period (mm)*	*X Phase (rad)*	*Y Period (mm)*	*Y Phase (rad)*	*X/Y Rotation (deg)*
a	0.045	3.674	3.271	3.746	-0.827	1.217
b	0.134	4.951	1.750	5.114	-0.999	1.302
c	0.208	6.681	3.624	6.795	-0.105	0.767
d	0.212	10.013	-4.250	10.166	-4.285	0.557
e	0.206	15.038	7.510	15.182	7.582	1.028

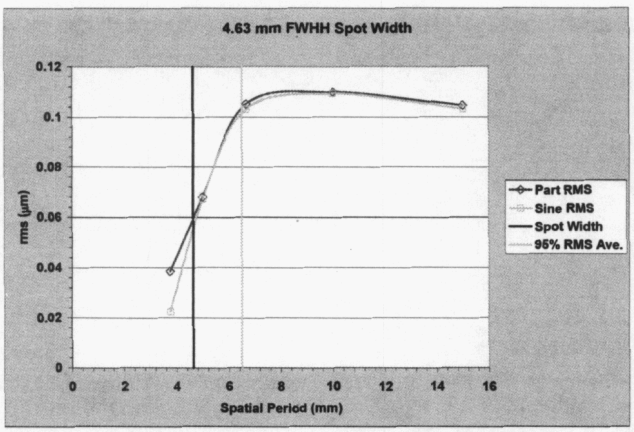

Figure 7: Computed and measured rms's for the imprints as a function of spatial period. Quality is high for large spatial periods. Rms deviates from its expected value as the topographical spatial period approaches the spot size. Taking 5 % deviation in the average rms as a metric on the imprints performed with small spots, a critical spot size of 7/10 (~2/3) the spatial period is obtained.

Fitting the experimental surface topography to the model two-dimensional sinusoidal pattern indicates that the spatial accuracy of the process is good within the interferometric lateral resolution of 0.133 mm/pixel (see Table 4). This observation holds for all the imprints. The model fits also indicate that the imprinting process becomes inefficient with loss in imprinting amplitude as the spatial period decreases. The imprinting errors, like in the constant period experiments, are composed mainly of topographical departures in the peak and valley areas.

The imprinted pattern falls short of the desired imprint depth under single pass conditions, Table 5. The accuracy, however, is high and closely represents the model surfaces. For the cases where the spatial periods are greater than the removal function dimensions, the difference between the prescription and the actual surface topography is attributable to lower amount of material removed. If the desired depth were attained, the surface quality would be with 5-7 percent of that desired.

Table 5: Surface characteristics for the imprinted two-dimensional topographies and the characteristics of the numerically fit sinusoidal waves.

Imprint	*Part PV (μm)*	*Sine Wave PV (μm)*	*Part rms (μm)*	*Sine Wave rms (μm)*
a	0.299	0.089	0.0385	0.0224
b	0.339	0.268	0.0680	0.0672
c	0.474	0.415	0.1052	0.1031
d	0.482	0.425	0.1098	0.1093
e	0.453	0.411	0.1046	0.1032

The rms for each of the imprints forms a trend in a fashion similar to that observed in the complementary experiment. As a function of spatial period (Figure 7), this metric remains high for spatial periods 15.0-, 10.0-, and 6.67-mm, and deteriorates at 5.0- and 3.75-mm spatial period. Invoking the same assumptions as before, that imprinting is satisfactory

to 95 percent of its average rms value, for the large spatial periods, 15.0-, 10-, and 6.67-mm, the intersection of this point and the spatial period on the plots yields an effective removal function size that is about 70 percent of the spatial period which is nearly the "two-thirds rule" previously identified.

CONTINUOUS PHASE PLATE IMPRINTING

One of the goals of the diagnostic experiments was to determine the ability of MRF to manufacture CPP's for NIF applications. The majority of the CPP's that will be used on NIF involve imprinting on large-aperture fused silica optics measuring 440 mm by 450 mm. These optics will be placed in the final optics assembly portion of the NIF beamlines and will operate in either 1ω or 3ω positions. Imprinting the large-aperture CPP's will require specialized MRF instruments capable of imprinting topographies on large-aperture optics. The Q22-Y MRF used in the present experiments cannot be used for large aperture work; however, the knowledge gained from experiments on small parts show that the MRF is capable of performing to the desired level needed for manufacture of large-aperture NIF CPP's. A limited set of small-aperture CPP's can be placed in the seed laser portion of the NIF system to provide some desired far-field spots at target chamber center for certain NIF experiments. These CPP's are 76 x 76 mm in size and can be manufactured using the Q22-Y MRF.

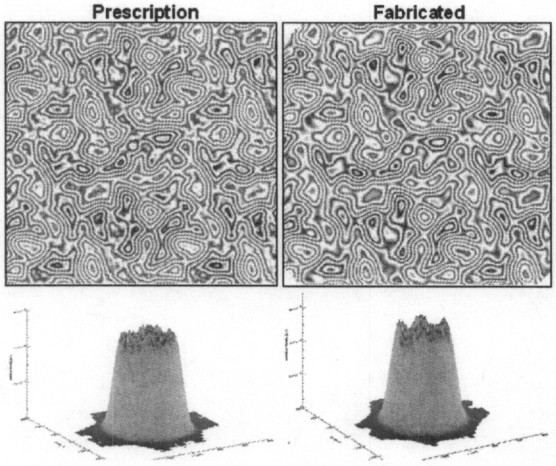

Figure 8: Phase front and computed far-field spot for miniature 0.5 mm NIF-CPP fabricated using MRF. The CPP prescription is shown on the left and the fabricated part is shown on the right.

The phasefront prescription for a the small-aperture NIF-CPP that was manufactured using MRF is shown in Figure 8. Its specified performance parameters are presented in Table 6. This prescription is a miniaturized version of a large-aperture CPP, which is scaled down by a factor of 8.27 that fills a 76 x 76 mm fused silica optic. All the topographical content in the large-aperture pattern is conserved in the miniaturized CPP prescription. When the seed laser beam is magnified through a relay telescope into the main laser beam line, the CPP produces a 0.5-mm far-field spot at the target plane when combined with a 770-cm focusing element.

MRF imprinting of this CPP incorporates the developments and observations made during the diagnostic studies. First, the imprinting utilizes a multi-pass approach to obtain the desired topographical fidelity. Second, each MRF pass incorporates a different removal function size that maximizes material removal over the topographical frequencies being imprinted. Larger removal functions are used early in the fabrication and small removal functions are used to perform final topographical correction. Third, in-process interferometry is used to track imprinting progress and to optimize phasefront corrections. Fourth, superposition is used during imprinting to provide for process breakpoints necessary for testing.

Table 6: Design specifications and measured values for the miniature NIF-CPP manufactured using MRF

	Specification	*Measured*	*Pass/Fail*
Radial Profile Super Gaussian Order	>10	11.6	PASS
Radial Profile Super Gaussian R0 (mm)	N/A	245.9	N/A
80% Encircled Energy Radius (mm)	213.0 +/- 15.0	212.9	PASS
90% Encircled Energy Radius (mm)	230.0 +/- 15.0	233.9	PASS
95% Encircled Energy Radius (mm)	245.0 +/- 15.0	250.5	PASS
Individual Lineout RMS Deviation (%)	7.0	5.1	PASS
2D RMS Deviation over Central Area (%)	7.0	5.7	PASS
Ellipticity (a = 237.8, b = 239.3)	1.0 +/- 0.1	1.0	PASS

The fabricated CPP imprinted onto a 76-mm piece of fused silica is also shown in Figure 8. The imprint was accomplished using two MRF removal function sizes, 3.4 mm and 1.1 mm (FWHH), in 2 passes and took 17 machine hours to imprint. The completed CPP passes all design specifications indicated in Table 6. We have since fabricated 8 small-aperture CPP's that were successfully used in NIF experimental campaigns: four CPP's with 0.5 mm far-field spot capability and four providing 1.0-mm far-field spots at the target plane. It is interesting to note that the topographical structure imprinted onto these small-aperture CPP's gives an indication of what can be done on large-aperture parts. If the topographical structure on a large-aperture optic is reproduced at the same spatial scale as used for the small-aperture parts, far-field spots in the neighborhood of 4.1- and 8.3-mm diameter can be realized at the target plane. This inference results from the demagnification used on the small-aperture CPP's. Overall, we have found that the unique deterministic-sub-aperture polishing characteristics of MRF make it possible to imprint complex topographical information onto optical surfaces at spatial scale-lengths approaching 1 mm regardless of the size of the optic.

7. Conclusions

In this study, MRF was used for the first time to accurately modify surface topography of glass surfaces in order to assess the process for the manufacture of CPP's for NIF. The accuracy of the MRF process to deterministically imprint patterns onto silica surfaces was tested with a representative set of prescribed topographical functions. The numerical and experimental results demonstrate that the manufacturing efficiency (i.e. the ability to imprint surface profiles as accurately and quickly as possible) is directly tied to the physical dimension of the removal function (width and length of the removal function). The study uncovered the advantages of using removal functions that are smaller than the feature to be imprinted. The FWHH of the removal function is found to be a good metric for predicting the quality or accuracy of the imprinted surface profile. The FWHH removal function size should be at least two-thirds smaller than the minimum spatial period to be imprinted onto the surface. The finite size of interaction area between the MR fluid and the workpiece leads to "collateral" polishing while the surface travels over the ribbon. The polishing time is mostly dependent on the amount of material that is removed because of this "collateral" polishing effect. As a result, the manufacturing efficiency can actually increase using lower material removal rates. Polishing time also directly scales with the topographical depth for a particular removal function size. Overall, MRF's unique deterministic-sub-aperture polishing characteristics make it possible to imprint complex topographical information onto optical surfaces at spatial scale-lengths approaching 1mm with excellent accuracy.

Several developments and observations were made during the diagnostic studies that lead to a process that could be used to imprint CPP's. First, imprinting should utilize a multi-pass MRF approach to obtain the desired topographical fidelity. Each pass should incorporate a different removal function size that maximizes material removal over the topographical frequencies being imprinted. Larger removal functions need to be used early in the fabrication process and small removal functions need to be used to perform final topographical correction. In-process interferometry should be an integral part of the process to optimize phasefront corrections. Superposition should be used during imprinting to provide for prescription simplification and process breakpoints necessary for testing.

ACKNOWLEDGEMENTS

The authors would like to acknowledge the support of Andrea Flammini in preparing this. This work was performed under the auspices of the U. S. Department of Energy by the University of California, Lawrence Livermore National Laboratory under Contract No. W-7405-Eng-48.

REFERENCES

[1]W.H. Lowdermilk. *Status of the National Ignition Facility project.* Solid State Lasers for Application to Inertial Confinement Fusion: Second Annual International Conference, M.L. Andre, ed., Proc. SPIE 3047, pp. 16-37 (1996).

[2]S.N. Dixit, M.D. Feit, M.D. Perry, and H.T. Powell. *Designing fully continuous phase screens for tailoring focal-plane irradiance profiles.* Optics Letters, vol. 21, no. 21, 1 Nov. 1996, pp. 1715-1717.

[3]B.W Woods, I.M. Thomas, M.A. Henessian, S.N. Dixit, H.T. Powell . *Large-aperture (80-cm diameter) phase plates for beam smoothing on Nova.* Solid State Lasers II, G.Dube, ed., Proc. SPIE 1410, pp. 47-54 (1991).

[4]S.N. Dixit, I.M. Thomas, B.W Woods, A.J. Morgan, M.A. Henessian, P.J. Wegner, and H.T Powell. *Random phase plates for beam smoothing on the Nova laser.* Applied Optics, 32, 2543-2554 (1993).

[5]I.M. Thomas, S.N. Dixit, and M.C. Rushford. *Kinoform phase plates for focal plane irradiance profile control.* Optics Letters, vol. 19, pp. 417-419 (1994).

[6]I.M. Thomas, S.N. Dixit, and M.C. Rushford. *Preparation of random phase plates for laser beam smoothing.* Laser Induced Damage in Optical Materials: 1994 H.E. Bennett A.H. Guenther, M.R. Kozlowski, B.E. Newman and M.J. Soileau, eds., Proc. SPIE 2428, pp. 264-270 (1994).

[7]*Distributed phase plates for super-Gaussian focal plane irradiance profiles.* LLE (Laboratory for Laser Energetics) Rev. 63, pp. 126-129 (1995).

[8]Jerome Neauport, Xavier Ribeyre, Jerome Daurios, Denis Valla, Martine Lavergne, Vincent Beau, and Laurent Videau. *Design and optical characterization of a large continuous phase plate for Laser Integration Line and laser Megajoule facilities.* Applied Optics, vol. 42, no. 13, 1 May 2003, pp. 2377-2383.

[9]Joseph A. Menapace, Bernie Penetrante, Don Golini, Al Slomba, Phil E. Miller, Tom Parham, Mike Nichols, and John Peterson. *Combined advanced finishing and UV-laser conditioning for producing UV-damage-resistant fused silica optics.* Laser Induced Damage in Optical Materials: Proc. SPIE, 4679, pp. 56-68 (2001).

[10]US Patents covering the MRF technology: 5,449,319; 5,525,249; 5,577,948; 5,795,212; 5,804,095; 5,839,944; 5,951,369; 6,106,380.

[11]Zhang Feng, Zhang Xuejun, Yu Jingchi. *Mathematics model of magnetorheological finishing.* SPIE - Int. Soc. Opt. Eng. Proceedings of SPIE - the International Society for Optical Engineering, vol. 4231, 2000, pp. 490-7.

[12]Pollicove HM. *Next-generation optics manufacturing technologies.* SPIE-Int. Soc. Opt. Eng. Proceedings of SPIE - the International Society for Optical Engineering, vol. 4231, 2000, pp. 8-15.

[13]Shorey AB, Jacobs SD, Kordonski WI, Gans RF. *Experiments and observations regarding the mechanisms of glass removal in magnetorheological finishing.* Applied Optics, vol. 40, no.1, 1 Jan. 2001, pp. 20-33.

[14]Kordonski WI, Golini D. *Fundamentals of magnetorheological fluid utilization in high precision finishing.* Journal of Intelligent Material Systems & Structures, vol.10, no.9, Sept. 1999, pp. 683-9.

[15]S.R. Arrasmith, I.A. Kozhinova, L.L. Gregg, A.B. Shorey, H.J. Romanofsky, S.D. Jacobs, D. Golini, W.I. Kordonski, S.J. Hogan, P. Dumas, *Details of the polishing spot in magnetorheological finishing (MRF)*, SPIE - Int. Soc. Opt. Eng. Proceedings of SPIE - the International Society for Optical Engineering, vol. 3782, 1999, pp. 92-100.

[16]S.D. Jacobs, Yang Fuqian, E.M. Fess, J.B. Feingold, B.E. Gillman, W.I. Kordonski, H. Edwards, D. Golini, *Magnetorheological finishing of IR materials*, SPIE-Int. Soc. Opt. Eng. Proceedings of SPIE - the International Society for Optical Engineering, vol. 3134, 1997, pp. 258-69.

[17]W. Kordonski, S. Jacobs, *Model of magnetorheological finishing, Sixth International Conference on Adaptive Structures*, Technomic Publishing, 1996, pp. 63-74. Lancaster, PA.

[18]D. Golini, W.I. Kordonski, P. Dumas, S.J. Hogan, *Magnetorheological finishing (MRF) in commercial precision optics manufacturing*, SPIE-Int. Soc. Opt. Eng. Proceedings of SPIE - the International Society for Optical Engineering, vol.3782, 1999, pp. 80-91.

[19]S.D. Jacobs, D. Golini, Y. Hsu, B.E. Puchebner, D. Strafford, W.I. Kordonski, I.V. Prokhorov, E. Fess, D. Pietrowski, V.W. Kordonski. *Magnetorheological finishing: a deterministic process for optics manufacturing*, SPIE-Int. Soc. Opt. Eng. Proceedings of SPIE - the International Society for Optical Engineering, vol. 2576 (1995), pp. 372-82.

[20]Surface Texture (Surface Roughness, Waviness, and Lay), ANSI/ASME B46.1 (1985), American Society of Mechanical Engineers, New York.

[21]Q22 MRF System Manual, QED Technologies, Part Number MAN5006-B Manual, Q22-P MRF System, STD.

[22]John Neter, William Wasserman, G. A. Gilmore, *Applied Statistics*, Allyn and Bacon, Boston (1978), p. 63.